Engineering Structures 114 (2016) 61–74

Contents lists available at ScienceDirect

Engineering Structures

journal homepage: www.elsevier.com/locate/engstruct

Dynamic response of high speed vehicles and sustaining curved bridges under conditions of resonance

Qing Zeng [a], Y.B. Yang [b], Elias G. Dimitrakopoulos [a,*]

[a] Department of Civil and Environmental Engineering, The Hong Kong University of Science and Technology, Clear Water Bay, Kowloon, Hong Kong
[b] School of Civil Engineering, Chongqing University, Chongqing 400045, China

ARTICLE INFO

Article history:
Received 11 June 2015
Revised 3 February 2016
Accepted 3 February 2016

Keywords:
Vehicle-bridge-interaction
Curved bridge
Resonance
Cancelation
Railway bridge

ABSTRACT

This paper examines the dynamic response of *vehicle(s)* moving at high speeds and the sustaining horizontally *curved (simple, continuous or multi-unit) bridges*, when each subsystem is set into resonance. The bridge is simulated by finite elements and each vehicle as a multibody system. The coupling contact forces, between the vehicle and the bridge, are derived by adopting a rigid contact assumption. Key feature of the present study is the simulation of the three-dimensional (3D) dynamics of a vehicle running over a horizontally curved path. This simulation allows the examination of deformation modes of the 3D multibody vehicle model (e.g. related to lateral-rolling and yawing degrees of freedom) for the first time. In all cases, the numerical results agree well with pertinent analytical solutions. From the parametric study, the followings are observed: (1) The impact factors show the same pattern for the vertical and the radial directions. (2) The suspension damping can alleviate the resonance response of the car body even when the vehicle's resonance condition is met. (3) The feedback effect of the bridge's resonance to the vehicle response is large, but the vehicle's resonance effect on the bridge response is quite small, especially along the vertical direction. (4) No resonance of the middle span of the continuous bridge occurs for the second mode in the vertical and the radial directions. (5) The increase in the number of spans results in both smaller displacement and lower impact factor.

1. Introduction

During the passage of a train over a bridge, the bridge resonance vibration occurs when the loading frequency of the moving vehicles coincides with a natural frequency of the bridge [1,2]. The intense vibrations induced by the bridge resonance, affect not only the serviceability and the life span of the bridge, but also reduce the running safety of the trains and the comfort of passengers [2,3]. On the other hand, when the bridge cancelation occurs, the free vibrations induced by the moving vehicles sum up to zero, leaving practically, no or little, residual response on the bridge after the last wheel load of the train leaves the bridge [1,2]. The cancelation effect may suppress the vibration of the bridge even when the resonance condition is met, which is favorable for the working state of the bridge, running safety of the vehicle, and riding comfort of the passengers [1,2].

Yang et al. [1] studied the resonance and the cancelation conditions of a simply supported straight beam, by modeling the vehicles as a series of equidistant moving loads. They proposed optimal design criteria for bridges according to the derived conditions of resonance and cancelation. Further, Yau et al. [4] and Yang et al. [5] investigated the resonance and the cancelation mechanism of a simply supported bridge with elastic supports in the vertical direction. The vibration shape of the elastically supported beam was modeled by the superposition of a flexural sine mode and a rigid body mode. They indicated that the resonance speeds were lower for elastically supported beams than those for simply supported beams. They also showed that the critical speed for cancelation to occur is independent of the support stiffness. Xia et al. [6] investigated the resonance mechanism of different bridge types using theoretical derivations, which were assessed by numerical simulations and field measurements. Also, Xia et al. [7] derived the solution for the resonant and cancelation vibrations of simple bridges under moving train loads, and confirmed the cancelation effect. Xia et al. [8] studied the lateral resonance condition of a 48-span straight simply-supported steel truss bridge, considering the wind pressures acting on vehicle bodies. Also, Song et al. [9] examined the resonance of a composite bridge and a box-girder bridge, while Ju and Lin [10] of an arch bridge and Yau and

* Corresponding author. Tel.: +852 2358 5975.
E-mail address: ilias@ust.hk (E.G. Dimitrakopoulos).

http://dx.doi.org/10.1016/j.engstruct.2016.02.006
0141-0296/

Frýba [11] of a suspension bridge. More resonance studies include: the theoretical approach of Frýba [12], the bridge-track-vehicle model by Cheng et al. [13] and the nonlinear wheel-rail analysis of Dinh et al. [14].

Yang et al. [15] derived the analytical solution for a horizontally curved beam subjected to vertical and horizontal moving loads, with the later generated by the centrifugal forces of vehicles moving over a circular path. They confirmed the results by an independent numerical simulation. This study was likely the first on the lateral resonance of curved bridges. Except those by Yang's group [2,3,16], most previous studies on resonance and cancelation focused mainly on the vertical resonance of straight bridges, with basically no evaluation of the performance of the vehicles under the conditions of bridge resonance. Recall that, the term *vehicle-bridge interaction* (VBI) was first introduced in 1995 [16] to emphasize the equal importance of the two subsystems: moving vehicles and bridges. When the loading frequency from the bridge coincides with the natural frequency of the vehicles constituting the train, the vehicular dynamic response is amplified (i.e. due to resonance) [8]. Recently, Yang and Yau [17] studied the vertical and the pitching resonances of vehicles moving over a series of simple beams, by considering the vehicle-bridge interaction of the *first-order*. Namely, the bridge response induced by the moving vehicles was included in evaluating the vehicles' response. Of course, the vehicles' response will affect the bridge again, but this is a *second-order* feedback, which is quite small and therefore was neglected. To the authors' knowledge, with the exception of [17], very few studies examined the resonance of the vehicle system, especially using a fully 3D multibody vehicle model, in particular the 3D resonance of the car body's motion for the lateral-rolling and the yawing degrees of freedom (DOFs).

The study of resonance in VBI systems offers a constructive guidance for the design of railway lines and has significant engineering implications. The critical conditions of the resonance should always be avoided in practical design [2]. Similarly, it is imperative to avoid the occurrence of the resonance when speeding-up existing railway lines over bridges [2]. To this end, an optimal speed for the train is the one that satisfies the condition of cancelation [2]. In this context, the primary scope for this study is: (i) to elucidate numerically the resonance and the cancelation conditions of horizontally curved railway bridges, including simply supported and continuous ones. In this context, the impact of the bridge resonance to the response of running vehicles is assessed; and (ii) to investigate numerically the resonance conditions of vehicles running over horizontally curved multi-span railway bridges and to examine the effect of vehicle resonance on the response of the supporting bridge.

2. Dynamic analysis of the vehicle-bridge interaction

2.1. Modelling of the vehicle and vehicular dynamics

As shown in Fig. 1, each vehicle of the train is modeled as a 3D multibody assembly, consisting of one car body, two bogies and four wheelsets. The distinct components, the car-body, the bogies and the wheelsets, are rigid (non-deforming) bodies connected by linear springs and viscous dashpots representing the suspension system.

To describe the motion of the vehicle running along a horizontally curved path, the present study employs three systems of reference: an inertial (space-fixed) system *I*, a *moving trajectory system TI*, and a body-fixed system *IR* (Fig. 2), following [18]. The motion of the *moving trajectory system* is defined by a time-dependent coordinate, the arc length s^i (Fig. 2). The longitudinal direction of the trajectory system $O^{ti}X^{ti}$ is set tangent to the curve at its origin O^{ti}. The orientation of the moving *trajectory system* is then defined using three Eulerian angles about the three axes

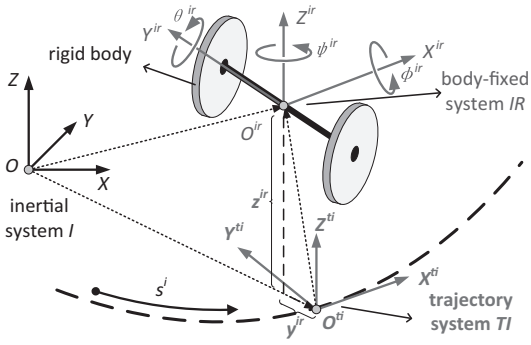

Fig. 2. Three coordinate systems used, adapted from [18].

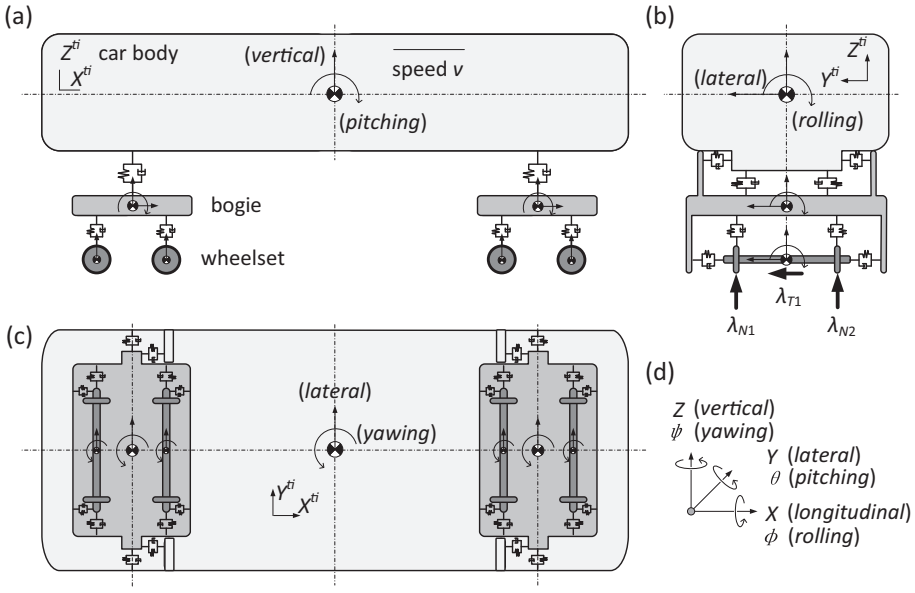

Fig. 1. Vehicle model: (a) side view, (b) back view, (c) top view, and (d) coordinate system.

Z^{ti}, X^{ti} and Y^{ti}, which are known functions of the arc length s^i. The body-fixed system follows the longitudinal motion of the trajectory system, with its origin fixed to the center of mass of the body. The motion of the rigid body in the trajectory coordinate system is described with five time-dependent coordinates: two translations y^{ir} (lateral) and z^{ir} (vertical), and three Eulerian angles ψ^{ir} (yawing), ϕ^{ir} (rolling) and θ^{ir} (pitching) about the three axes Z^{ir}, X^{ir} and Y^{ir}, respectively (Fig. 2).

The equation of motion for each vehicle, in the trajectory coordinate system, is:

$$\mathbf{M}^V(t)\ddot{\mathbf{u}}^V + \mathbf{C}^V\dot{\mathbf{u}}^V + \mathbf{K}^V\mathbf{u}^V - \mathbf{W}_N^V\lambda_N - \mathbf{W}_T^V\lambda_T = \mathbf{F}^V \tag{1}$$

where $\mathbf{K}^V$ and $\mathbf{C}^V$ are the stiffness and damping matrices, respectively, of the vehicle given in [19]; $\mathbf{M}^V(t)$ is the mass matrix of the vehicle, which is time-dependent due to the rotating system of reference [20]. Considering a specific rigid body component of the vehicle (indicated with a superscript i), for instance a wheelset in Fig. 2, the mass matrix is:

$$\mathbf{M}^i(t) = {}_I\mathbf{L}^i(t)^{\mathrm{T}} m_I^i {}_I\mathbf{L}^i(t) + {}_{IR}\mathbf{H}^i(t)^{\mathrm{T}} {}_{IR}\mathbf{I}^i_{\theta\theta IR} {}_{IR}\mathbf{H}^i(t) \tag{2}$$

Throughout this paper, the superscript "T" denotes the transpose of a matrix, and the left subscript denotes the reference system to which each vector or matrix is referring to; m^i is the lumped mass of the rigid body and ${}_{IR}\mathbf{I}^i_{\theta\theta}$ is the inertia tensor about the principal axes of rigid body i. The matrices ${}_I\mathbf{L}^i(t)$ and ${}_{IR}\mathbf{H}^i(t)$ are time-varying velocity transformation matrices, pertaining to the translational and the rotational DOFs, respectively, which arise due to the horizontally curved path [18].

In Eq. (1), $\mathbf{u}^V \in \Re^{31,1}$ is the displacement vector of the whole vehicle, where the symbol $\in \Re^{31,1}$ denotes a real matrix with 31 rows and 1 column. The car body and the bogies are assigned 5 DOFs (Fig. 1), with the acceleration vector $\ddot{\mathbf{u}}^u$ in terms of the trajectory coordinates TI:

$$\ddot{\mathbf{u}}^u = \begin{bmatrix} \ddot{y}^u & \ddot{z}^u & \ddot{\psi}^u & \ddot{\phi}^u & \ddot{\theta}^u \end{bmatrix}^{\mathrm{T}} \tag{3}$$

Each wheelset has 4 DOFs (Fig. 1),

$$\ddot{\mathbf{u}}^w = \begin{bmatrix} \ddot{y}^w & \ddot{z}^w & \ddot{\psi}^w & \ddot{\phi}^w \end{bmatrix}^{\mathrm{T}} \tag{4}$$

where the superscript $(\,)^u$ (Eq. (3)) stands for the upper part of the vehicle (car body and the bogie), and $(\,)^w$ (Eq. (4)) for the wheelset.

In Eq. (1), $\mathbf{F}^V$ is the force vector:

$$\mathbf{F}^V = \mathbf{F}_g^V + \mathbf{F}_v^V \tag{5}$$

where $\mathbf{F}_g^V$ is the gravitational force vector of the vehicle, and $\mathbf{F}_v^V$ is the inertial force vector – centrifugal forces and Coriolis forces due to the curved path. For a single rigid body i, the inertial force vector $\mathbf{F}_v^i$ (due to the curved path) is

$$\mathbf{F}_v^i = -m^i {}_I\mathbf{L}^i(t)^{\mathrm{T}} {}_I\boldsymbol{\gamma}_R^i - {}_{IR}\mathbf{H}^i(t)^{\mathrm{T}}\left({}_{IR}\mathbf{I}^i_{\theta\theta IR}{}_{IR}\boldsymbol{\gamma}^i_{\alpha} + {}_{IR}\boldsymbol{\omega}^i \times \left({}_{IR}\mathbf{I}^i_{\theta\theta IR}{}_{IR}\boldsymbol{\omega}^i\right)\right) \tag{6}$$

where ${}_{IR}\boldsymbol{\omega}^i$ is the angular velocity vector defined in the body-fixed system, while vectors ${}_I\boldsymbol{\gamma}_R^i$ and ${}_{IR}\boldsymbol{\gamma}_{\alpha}^i$ contain additional quadratic velocity terms, produced during the time-differentiation of the absolute translational and the absolute angular velocities, respectively [18].

In Eq. (1), λ_N and λ_T are the normal and the tangential contact force vectors, respectively (to be discussed in Section 2.3); $\mathbf{W}_N^V$ and $\mathbf{W}_T^V$ are the direction matrices of the corresponding contact forces λ_N and λ_T [20]. Throughout this paper, the subscripts N and T, respectively, stand for the normal and the tangential directions of contact. The only nonzero entries in matrices $\mathbf{W}_N^V$ and $\mathbf{W}_T^V$ correspond to the wheels of the vehicle. For the upper part of the vehicle, i.e., the car body and the bogies, the pertinent submatrices are zero [20].

2.2. Modelling of the bridge

The bridge is modeled by 3D Euler–Bernoulli beam elements, using linear and cubic (Hermitian) shape functions [21]. Six DOFs are considered per node: three translations and three rotations with respect to the X, Y and Z axes accordingly.

After assembly, the mass matrix $\mathbf{M}^B$ and the stiffness matrix $\mathbf{K}^B$ for the entire bridge are obtained in the global system. The damping matrix $\mathbf{C}^B$ is assumed to be of the Rayleigh type and calculated by setting the damping ratios of the first two modes to be 0.02 [21]. The equation of motion for the bridge is

$$\mathbf{M}^B\ddot{\mathbf{u}}^B + \mathbf{C}^B\dot{\mathbf{u}}^B + \mathbf{K}^B\mathbf{u}^B + \mathbf{W}_N^B\lambda_N + \mathbf{W}_T^B\lambda_T = \mathbf{F}^B \tag{7}$$

where $\mathbf{u}^B$ is the bridge displacement vector and $\mathbf{F}^B$ is the vector of the loads acting on the bridge; $\mathbf{W}_N^B$ and $\mathbf{W}_T^B$ are the contact force direction matrices for the bridge, which contain linear shape functions for the axial and torsional DOFs, and cubic (Hermitian) shape functions for the flexural DOFs. The only nonzero entries in the $\mathbf{W}_N^B$ and $\mathbf{W}_T^B$ matrices correspond to the DOFs of the bridge elements in contact with the wheels of the vehicle [20].

2.3. Modelling of interaction between the two sub-systems

To derive the coupled equation of motion for the VBI system, firstly the pertinent matrices and vectors of the two individual subsystems in the equations of motion are gathered as:

$$\mathbf{M}^*(t)\ddot{\mathbf{u}} + \mathbf{C}\dot{\mathbf{u}} + \mathbf{K}\mathbf{u} - \mathbf{W}\lambda = \mathbf{F} \tag{8}$$

where the global mass matrix $\mathbf{M}^*(t)$, global stiffness matrix $\mathbf{K}$ and global damping matrix $\mathbf{C}$ are

$$\mathbf{M}^*(t) = \begin{bmatrix} \mathbf{M}^V(t) & \mathbf{0} \\ \mathbf{0} & \mathbf{M}^B \end{bmatrix}, \quad \mathbf{C} = \begin{bmatrix} \mathbf{C}^V & \mathbf{0} \\ \mathbf{0} & \mathbf{C}^B \end{bmatrix}, \quad \mathbf{K} = \begin{bmatrix} \mathbf{K}^V & \mathbf{0} \\ \mathbf{0} & \mathbf{K}^B \end{bmatrix} \tag{9}$$

The contact direction matrices $\mathbf{W}_N$ and $\mathbf{W}_T$, the displacement vector $\mathbf{u}$ and the force vector $\mathbf{F}$ for the whole system are constructed in an analogous manner:

$$\begin{cases} \mathbf{u} = \begin{bmatrix} \mathbf{u}^V \\ \mathbf{u}^B \end{bmatrix}, \quad \mathbf{F} = \begin{bmatrix} \mathbf{F}^V \\ \mathbf{F}^B \end{bmatrix}, \quad \lambda = \begin{bmatrix} \lambda_N \\ \lambda_T \end{bmatrix}, \\ \mathbf{W} = \begin{bmatrix} \mathbf{W}_N & \mathbf{W}_T \end{bmatrix}, \quad \mathbf{W}_N = \begin{bmatrix} \mathbf{W}_N^V \\ -\mathbf{W}_N^B \end{bmatrix}, \quad \mathbf{W}_T = \begin{bmatrix} \mathbf{W}_T^V \\ -\mathbf{W}_T^B \end{bmatrix} \end{cases} \tag{10}$$

A key to solving the VBI problem is the treatment of the coupling contact forces. The present study adopts a "*rigid contact*" approach, and calculates a set of equivalent contact forces per wheelset, considering two contact forces per wheelset (i.e. one per wheel) in the normal direction, and one contact force in the tangential direction (the resultant of the contacts at the two wheels) in Fig. 1b [20]. The "*rigid contact*" approach assumes no separation/uplifting in the normal direction and no sliding in the tangential direction. On the acceleration level, this kinematic constraint implies that the relative acceleration $\ddot{\mathbf{g}}$ between the wheel and the rail is zero [20]:

$$\ddot{\mathbf{g}} = \mathbf{W}^{\mathrm{T}}\mathbf{M}^*\mathbf{h} + \mathbf{G}\lambda + \bar{\mathbf{w}} = \mathbf{0} \tag{11}$$

where matrix $\mathbf{G}$ is equal to $\mathbf{G} = \mathbf{W}^{\mathrm{T}}\mathbf{M}^{*-1}\mathbf{W}$, and its inverse $\mathbf{G}^{-1}$ represents the mass activated by the contact interaction. The vector $\mathbf{h}$ contains all non-contact forces:

$$\mathbf{h} = \mathbf{F}(t) - \mathbf{C}\dot{\mathbf{u}} - \mathbf{K}\mathbf{u} \tag{12}$$

and $\bar{\mathbf{w}}$ (Eq. (13)) is the vector of the additional generalized velocity terms [20]:

$$\bar{\mathbf{w}} = 2v\mathbf{W}'^{\mathrm{T}}\dot{\mathbf{u}} + v^2\mathbf{W}''^{\mathrm{T}}\mathbf{u} \tag{13}$$

where $(\,)'$ denotes differentiation with respect to the arc length s^i. Eqs. (12) and (13) allow the calculation of the contact forces vector $\boldsymbol{\lambda}$:

$$\boldsymbol{\lambda} = -\mathbf{G}^{-1}\left(\mathbf{W}^{\mathrm{T}}\mathbf{M}^{*-1}\mathbf{h} + \bar{\mathbf{w}}\right) \tag{14}$$

Therefore, the equation of motion for the coupled vehicle-bridge system becomes

$$\mathbf{M}^*(t)\ddot{\mathbf{u}}(t) + \mathbf{C}^*(t)\dot{\mathbf{u}}(t) + \mathbf{K}^*(t)\mathbf{u}(t) = \mathbf{F}^*(t) \tag{15}$$

with

$$\begin{cases} \mathbf{C}^*(t) = \left[\mathbf{E} - \mathbf{W}(t)\mathbf{G}(t)^{-1}\mathbf{W}^{\mathrm{T}}(t)\mathbf{M}^*(t)^{-1}\right]\mathbf{C} + 2v\mathbf{W}(t)\mathbf{G}(t)^{-1}\mathbf{W}'^{\mathrm{T}}(t) \\ \mathbf{K}^*(t) = \left[\mathbf{E} - \mathbf{W}(t)\mathbf{G}(t)^{-1}\mathbf{W}^{\mathrm{T}}(t)\mathbf{M}^*(t)^{-1}\right]\mathbf{K} + v^2\mathbf{W}(t)\mathbf{G}(t)^{-1}\mathbf{W}''^{\mathrm{T}}(t) \\ \mathbf{F}^*(t) = \left[\mathbf{E} - \mathbf{W}(t)\mathbf{G}(t)^{-1}\mathbf{W}^{\mathrm{T}}(t)\mathbf{M}^*(t)^{-1}\right]\mathbf{F}(t) \end{cases} \tag{16}$$

where $\mathbf{E}$ is the identity matrix. Note that the mass matrix, the stiffness matrix, the damping matrix and the loading vector of the coupled system are all time-dependent [20].

3. Review of conditions of resonance and cancelation of the interacting vehicle-bridge system

3.1. Resonance of a simply supported bridge

According to Yang et al. [2], the critical vehicle speed for the resonance condition of a simply supported bridge is

$$v^B_{res,n,i} = 3.6\frac{f^B_n d^V}{i}\ \mathrm{km/h}, \text{with } i = 1,2,3\ldots \tag{17}$$

where f^B_n is the bridge frequency of the nth mode in Hz and d^V is the length of each vehicle. The critical vehicle speed of the bridge resonance in Eq. (17) is not directly affected by the span length of the bridge. A particular goal of this study is to verify that Eq. (17) is not only applicable to simply supported bridges, but also to other types of bridges, i.e., continuous bridges.

The critical speed for the cancelation of a simply supported bridge is calculated as [2]:

$$v^B_{can,n,i} = 3.6\frac{2f^B_n L^B}{2i-1}\ \mathrm{km/h}, \quad \text{with } i = 2,3\ldots \tag{18}$$

where L^B is the span length of the simply supported bridge.

3.2. Resonance of train vehicles

According to Yang and Yau [17], the critical speed of the vehicle resonance for a train traveling over a series of simply supported beams is

$$v^V_{res,n,i} = 3.6\frac{f^V_n L^B}{i}\ \mathrm{km/h}, \quad \text{with } i = 1,2,3\ldots \tag{19}$$

where f^V_n is the frequency of the vehicle of the nth mode.

3.3. Optimal design criterion

Once the conditions of cancelation are met, the resonance peak can be effectively suppressed, even when the conditions of resonance are satisfied [2]. Based on the phenomena of cancelation, Yang et al. [2] proposed an optimal bridge span/car length ratio which suppresses the resonance response:

$$\frac{L^B}{d^V} = i - 0.5, \quad \text{with } i = 2,3\ldots \tag{20}$$

where i is an integer denoting the order of cancelation, as in Eq. (18). Hence, given the vehicle length d^V of a specific train model, the designer can determine the optimal span length L^B of the bridge. Furthermore, when the span length is interpreted as the characteristic length [22], the optimal criterion, being independent of the train speed, can be applied to a wide range of simple and continuous beams. A particular goal of this study is to extend the optimal criterion Eq. (20) to more types of resonance, e.g. in the radial direction, aside from the vertical direction (see Figs. 4 and 5 later on).

4. Parametric study and discussions of the results

4.1. Single-span curved simply supported bridges subjected to a series of moving vehicles

This section deals with the resonance of single-span horizontally curved simply supported bridges subjected to a series of moving vehicles. The focus is on the response of both the bridge and the fully 3D moving vehicles under the bridge resonance condition. Fig. 3 shows a series of (ten) identical vehicles running over a single-span horizontally curved simply supported bridge. The properties assumed for the curved bridge of a single-line railway are: Young's modulus E = 28.25 GPa, mass per unit length m = 22.40 t/m, flexural moment of inertia $I_{zz} = 8.75\ \mathrm{m}^4$ in the lateral direction, and $I_{yy} = 4.11\ \mathrm{m}^4$ in the vertical direction, torsional constant J = 12.87 m^4, length of each span $L^B = 32$ m [23], and radius of the curvature R = 5000 m.

Based on the modal analysis of the finite element model, the natural frequencies of the bridge are 3.49 and 5.09 Hz for the vertical and the lateral direction, respectively. The length of the vehicle considered is $d^V = 25$ m. Therefore, according to Eq. (17), the predicted critical speeds v of the bridge resonance in the vertical and the radial directions are 314 and 458 km/h, respectively. Meanwhile, the predicted critical speeds of the bridge cancelation in the vertical and the radial directions are 268 km/h and 391 km/h, respectively (Eq. (18)). Fig. 4 shows the time history response of the vehicle-bridge system (of Fig. 3) as calculated with the proposed simulation approach. The symbol e.g. $v^B_{res/can,n,i}$ in Fig. 4 denotes the critical speed corresponding to n^{th} mode of the bridge and i^{th} order of the resonance/cancelation, as in Eqs. (17) and (18). It can be seen that the analytically predicted critical vehicle speeds, indeed cause the bridge resonance and the bridge cancelation. Fig. 4e and f also show that, under either the vertical or the radial resonance of the bridge, the later the vehicle enters the bridge, the higher the amplification of acceleration it sustains, due to the accumulated vibration of the bridge; an observation consistent with the results of Ref. [1].

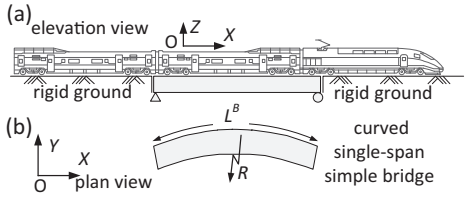

Fig. 3. Single-span horizontally curved simply supported bridges subjected to a series of moving vehicles.

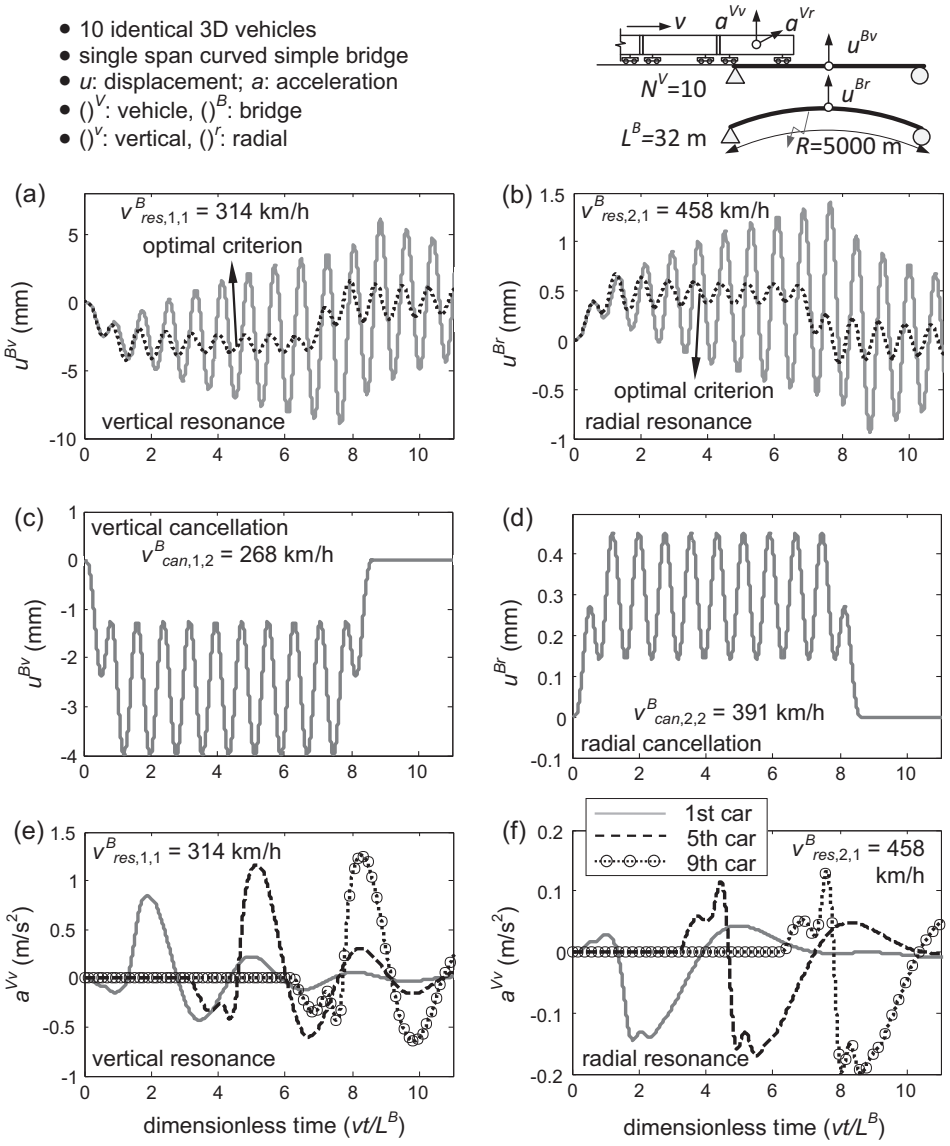

Fig. 4. Time history response computed by VBI analysis for 10 identical vehicles moving over a single-span curved simple bridge: (a), (c) and (e) vertical direction; (b), (d) and (f) radial direction; (a)–(d) displacement of the midpoint of the bridge; (a) and (b) resonance; (c) and (d) cancelation; and car-body acceleration of vehicles under (e) the vertical and (f) the radial resonance.

According to the optimal design criterion of Eq. (20), when $i = 2$, the optimal span/car length ratio is 1.5. Given the span length is 32 m, the optimal car length is $d^V = 32/1.5 = 21.33$ m. The black dotted lines in Fig. 4 (a and b) show the response of the bridge when the optimal design criterion (of cancelation) is met (i.e. d^V and L^B satisfy Eq. (20)). Observe that no resonance response occurs (in the vertical or the radial direction) even though the vehicles travel over the bridge at the critical resonance speed (Fig. 4a and b).

Fig. 5 depicts the effect of vehicle speed v on the response of the bridge in dimensional and dimensionless terms. Both the vertical displacement (Fig. 5a) and the radial displacement (Fig. 5c) of the midpoint of the bridge rise up drastically in the vicinity of the critical speeds, due to the resonance induced by the repetitive vehicular loading. As expected, the vertical displacement is not affected by the radius of the curved bridge, and the time histories for different bridge-radii collapse to a single curve (Fig. 5a). In general, the effect of the centrifugal force can be broken down to a quasi-static part and a dynamic part. The quasi-static effect of the centrifugal force can be inferred from a comparison of the dimensional with the dimensionless response (Fig. 5c vs. d). For increasing vehicle speed v, and a given radius R, the dimensional (radial) response displacement of the bridge shows an approximately parabolic pattern following the magnitude of the centrifugal forces $m^i v^2/R$. This parabolic pattern is disrupted by a peak at the dimensionless velocity $S^B = 0.78$, which can be attributed to the dynamic resonance. The dynamic effect is better understood through the dimensionless results (i.e., in terms of the impact factor Fig. 5d). When the response is scaled with respect to the (pseudo-static) effect of the centrifugal force, the dimensionless impact factor spectra in the radial direction, for different radii of curvature or different speeds, collapse to a single curve. Thus, these dimensionless spectra bring forward the dynamic effect of the centrifugal force and unveil a dynamic resonance precisely at the dimensionless speed predicted by the analytical methods. Some of the critical speeds appearing in Figs. 4 and 5 are 458 and

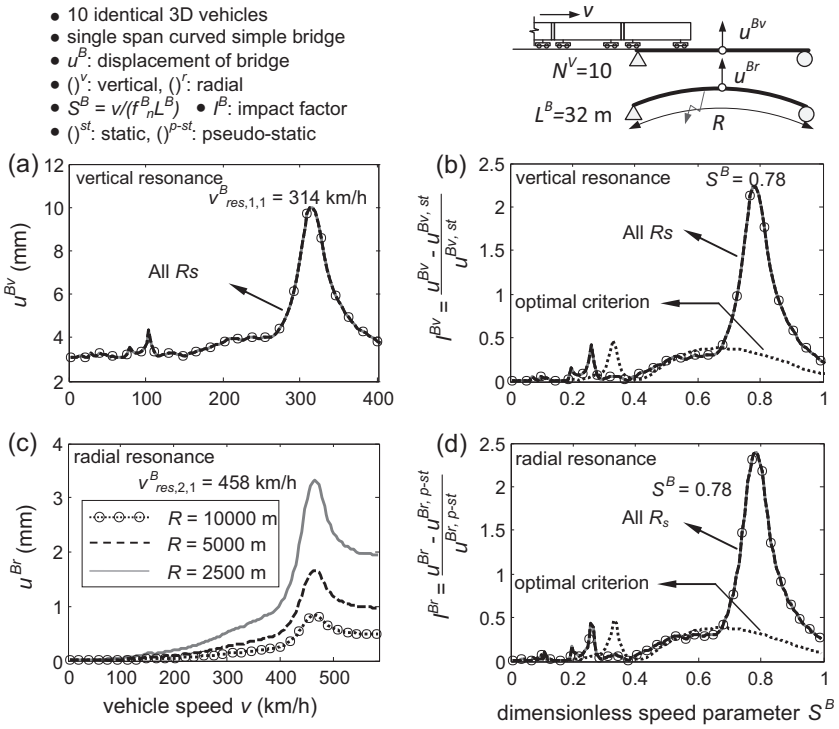

Fig. 5. Displacement response computed by the proposed VBI analysis for the midpoint of a simply supported curved beam subjected to ten identical vehicles: (a) and (b) vertical, (c) and (d) radial direction; (a) and (c) dimensional, (b) and (d) dimensionless response.

391 km/h. Note that the present results are valid provided that no hunting motion instability occurs. This limitation can be avoided using a more detailed contact model (see Zeng & Dimitrakopoulos [25]), which, though, is beyond the scope of the present study.

According to Yang et al. [2], the dimensionless speed parameter S^B of the bridge (Fig. 5b and d) is defined as the ratio of the excitation frequency of the moving vehicles to the frequency f_n^B of the bridge as

$$S^B = \frac{v}{f_n^B L^B} \tag{21}$$

where the excitation frequency of the moving vehicles is v/L^B, with L^B denoting the characteristic length of the bridge. The dimensionless impact factor I is [2]:

$$I = \frac{R_d(x) - R_s(x)}{R_s(x)} \tag{22}$$

where $R_d(x)$ and $R_s(x)$ are the peak dynamic and static displacements, respectively, of the bridge at the position x, due to the passage of the moving vehicles. In the vertical direction, $R_s(x)$ is calculated as the peak static displacement under the vehicle's weight. In the radial direction, $R_s(x)$ is taken as the peak pseudo-static response, calculated under the pseudo centrifugal force $m^i v^2/R$, where m^i is the lumped mass of the vehicle. The S^B value corresponding to the condition of resonance is [2]:

$$S^B = \frac{d^V}{L^B} \tag{23}$$

For a vehicle of length $d^V = 25$ m and a bridge of span $L^B = 32$ m, the resonant speed parameter computed from Eq. (23) is $S^B = 0.78$. Based on the present numerical analysis, the resonance speed parameters for the vertical (Fig. 5b) and the radial (Fig. 5d) directions agree well with the same predicted speed parameter $S^B = 0.78$. The dimensionless impact factors show the same pattern for the vertical and the radial directions of the bridge. Particularly, the dimensionless impact factor spectra in the radial direction collapse to a single curve for different radii of the bridge (Fig. 5d), as the centrifugal forces in the radial direction are determined by the combined effect of the radius of the curved bridge and the vehicle speed. The black dotted lines in Fig. 5b and d correspond to the optimal criterion in Eq. (20) by adjusting the vehicle length $d^V = L^B$ (32 m)/1.5 = 21.33 m. The first resonance peak response is suppressed when the optimal design criterion is satisfied (Fig. 5b and d).

4.2. Vehicles running on multi-unit horizontally curved simple bridge

In general, high-speed railway (HSR) bridges are short and with simple supports, yet, the length of the entire bridge system can be very long, consisting of a large number of bridge units. For instance, the 164 km Danyang-Kunshan Grand Bridge of the Beijing-Shanghai HSR line is the longest bridge system in the world [24], which contains over 4000 bridge units. In order to increase the efficiency of bridge construction, while reducing the cost of bridge manufacturing, usually the simply supported bridges and continuous bridges, adopted in the same railway lines, share the same standard span length [23]. Therefore, for each train vehicle traveling over a multi-unit bridge with the same span length (or characteristic length), the periodical excitation transmitted from the bridge may result in the resonance of the vehicle, if the excitation frequency coincides with a natural frequency of the vehicle. When in resonance, the dynamic response of the vehicle is amplified as the vehicle travels over more bridges (Fig. 6). This section extends the work of Yang and Yau [17] by studying the resonance of a single fully 3D vehicle moving over a multi-unit horizontally curved railway bridge. Importantly, the present analysis takes into account not only the vertical and the pitching DOFs

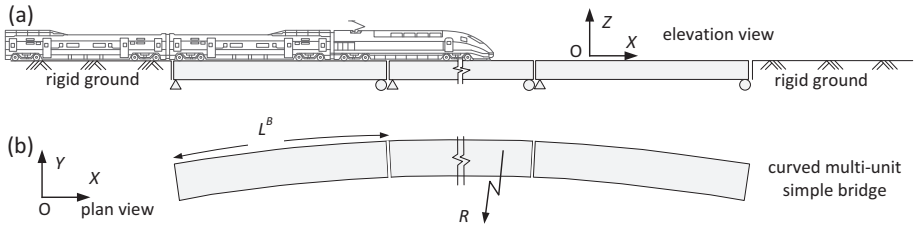

Fig. 6. A series of vehicles traveling over multi-unit horizontally curved simple bridge.

Table 1
Natural frequencies and critical resonance speeds from Eq. (19) for different vibration modes of the vehicle.

	$n = 1$	2	3	4	5
f_n^V (Hz)	0.54	0.78	0.90	1.43	1.60
Mode	Lateral–rolling	Lateral–rolling	Vertical	Yawing	Pitching
$v_{res,n,1}^V$ (km/h)	62	90	102	164	184

of the moving vehicles, but also the lateral and the rolling DOFs of the moving vehicles.

The proposed numerical analysis scheme is used to simulate one single train vehicle moving over a series of simple bridges/beams. The multi-unit bridge consists of 10 identical simply-supported curved units of span length 32 m and a constant radius of 5000 m. The material properties and section properties adopted are: Young's modulus $E = 28.25$ GPa, mass per unit length $m = 41.74$ t/m, flexural moment of inertia $I_{zz} = 74.42$ m^4 in the lateral direction, and $I_{yy} = 7.84$ m^4 in the vertical direction, and torsional constant $J = 15.65$ m^4 [2]. The vehicle model corresponds to the China-star high speed train [19]. Table 1 lists the first five natural frequencies and the corresponding vibration modes of the vehicle adopted, based on the modal analysis of the multibody vehicle system. Table 1 also summarizes the pertinent critical speeds, predicted from Eq. (19), which can trigger the vehicle resonance. Fig. 7 sketches the first five modes of the vehicle model.

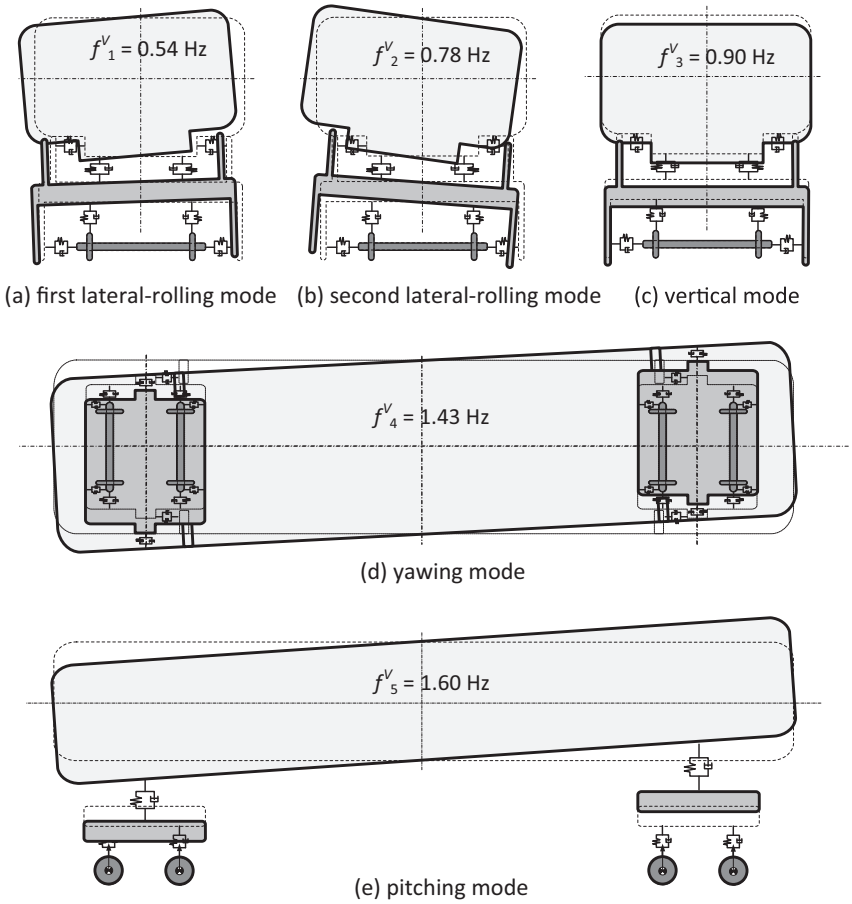

Fig. 7. Five vibration modes of the vehicle model adopted.

Fig. 8 shows the accelerations of the car body of the vehicle under the conditions of resonance for different modes of the vehicle. Again, the critical speeds in Fig. 8 agree well with the predicted analytical critical speeds listed in Table 1. When in resonance, the acceleration of the car body keeps increasing (for all five DOFs in Fig. 8) as the vehicle moves over more bridge units. Fig. 8 also investigates the effect of damping of the vehicle suspension system on the vehicle resonance response. In the legend of Fig. 8, the symbol C^V (the black dotted line) stands for the full damping value of the whole vehicle system with the data given in [19]. When the full damping is assumed, the response of the vehicle does not build up, even when the vehicle travels over more bridges under resonance. The resonance phenomena of the vehicle emerge only when the damping of the vehicle is reduced (e.g. to 10% of the full value C^V – the gray solid $0.1C^V$ line in Fig. 8). Consequently, the presence of damping in the suspension system prevents the resonance response of the car body to build up even when resonance conditions of the vehicle are met.

Fig. 9 shows the time histories of the bridge displacement of the midpoint of different spans induced by the vehicle's resonance. The points of interest are the midpoints of the 1st, the 5th, and the 9th span of the bridge. Fig. 9a, b and d shows the radial displacements of different spans of the bridge under the vehicle's lateral-rolling and yawing resonance. Fig. 9c and e show the vertical displacements of different spans of the bridge under the vehicle's vertical and pitching resonance. As revealed by Fig. 9a, b and d, under the vehicle's lateral-rolling and yawing resonances, the radial displacements of the later spans of the multi-unit bridge are slightly amplified due to the accumulated lateral vibrations of the vehicle. The amplification effect of the vehicle's resonance to the bridge response in the vertical direction (Fig. 9c and e) is marginal (of second-order), compared with that in the radial (lateral) direction. In general, it is concluded that the feedback effect of vehicle's resonance to the bridge response is quite small, particularly for the vertical direction.

Fig. 10 shows the accelerations for all five DOFs of the car body, i.e., lateral (radial), vertical, rolling, yawing and pitching, of the vehicle against the speed. The horizontal axis represents the dimensionless speed parameter S^V of the vehicle:

$$S^V = \frac{v}{f_n^V L^B} \tag{24}$$

All the considered DOFs reveal a coincident resonance speed parameter of $S^V = 1$. The critical speeds in Fig. 10 agree well with the analytical predictions given in Table 1. The pertinent accelerations are amplified in the vicinity of the resonance speeds. Particularly, the critical speed $v^V_{res,2,2} = 45$ km/h in Fig. 10a and $v^V_{res,3,2} = 51$ km/h in Fig. 10b are the second critical speeds, which are half of the first critical speeds $v^V_{res,2,1} = 90$ km/h and $v^V_{res,3,1} = 102$ km/h of the lateral resonance and the vertical resonance, respectively.

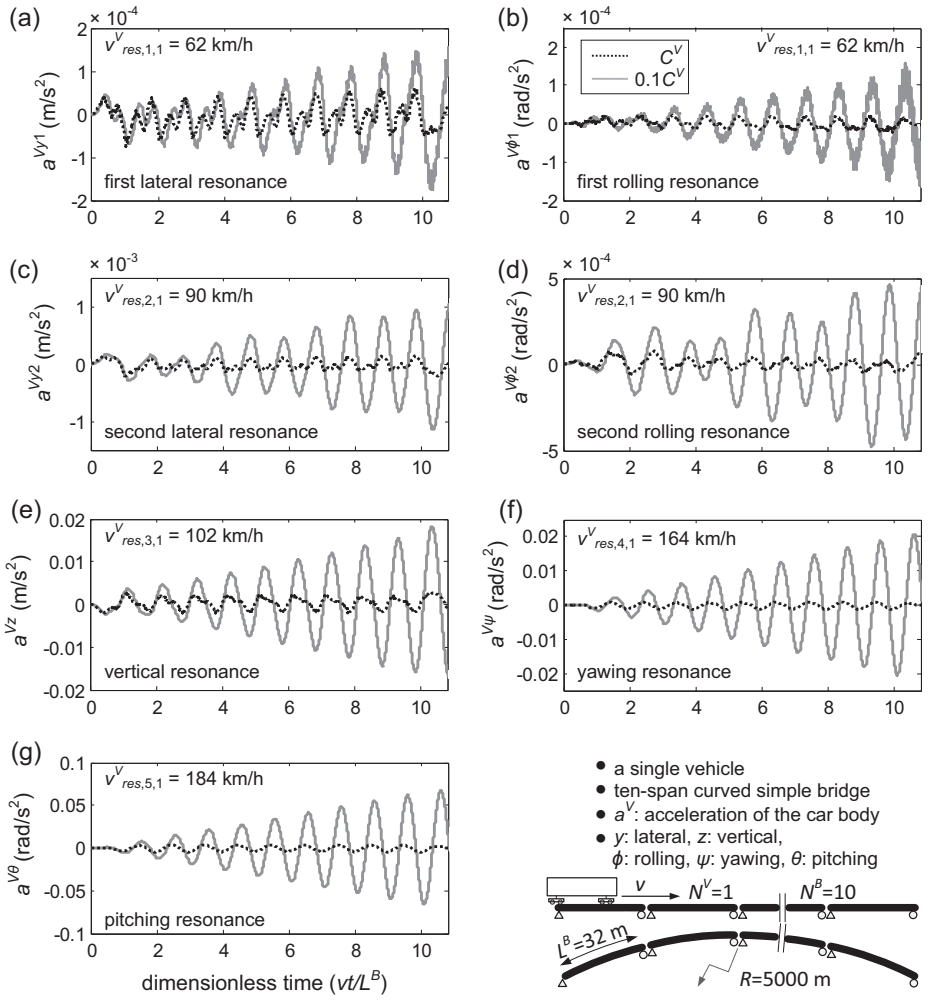

Fig. 8. Resonance response of the accelerations of the car body of the vehicle traveling over a multi-unit horizontally curved simple bridge: (a) the lateral, (b) the rolling, (c) the lateral, (d) the rolling, (e) the vertical, (f) the yawing and (g) the pitching accelerations.

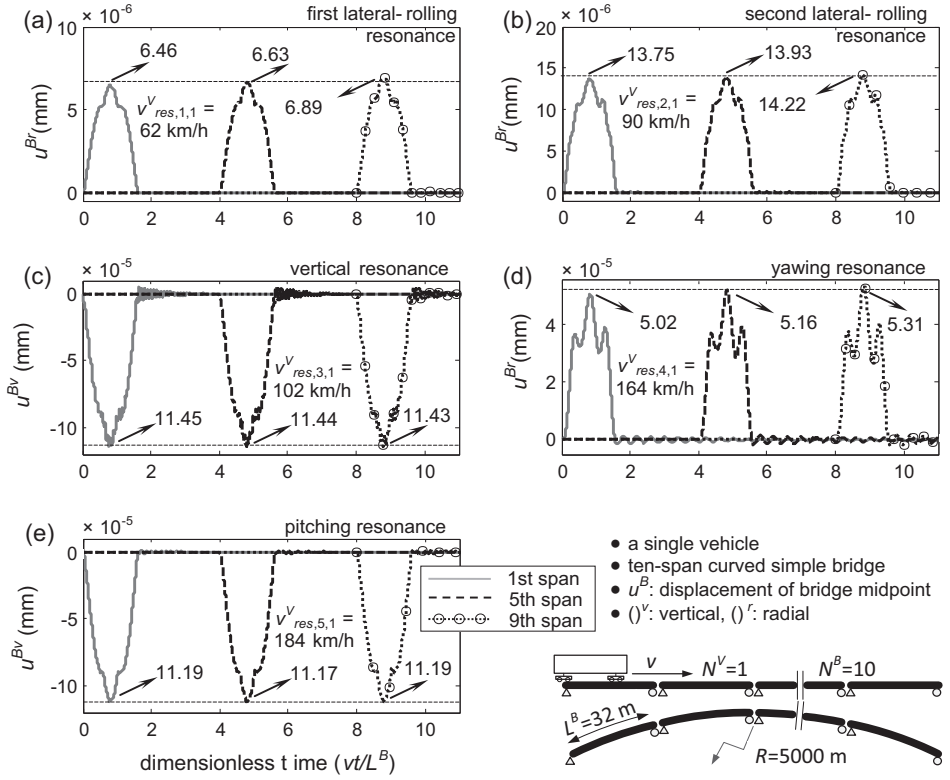

Fig. 9. Induced displacement time histories of the midpoint of different spans of the bridge under the conditions of vehicle resonance: (a) the radial, (b) the radial, (c) the vertical, (d) the radial and (e) the vertical displacements.

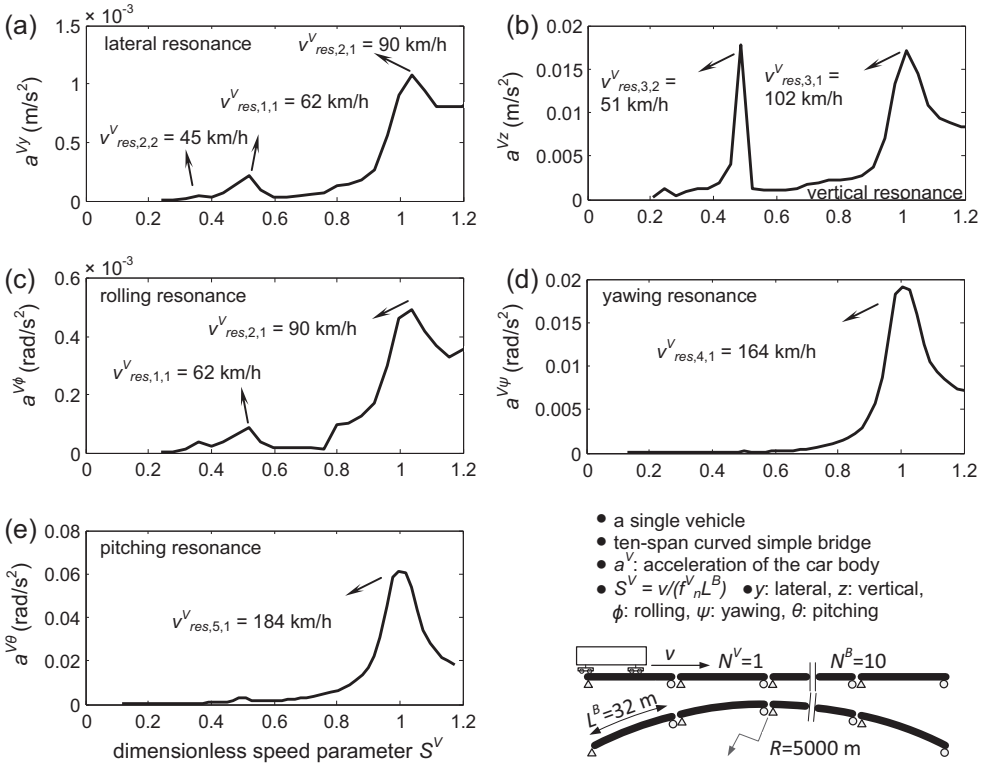

Fig. 10. Acceleration spectra vs. vehicle speed computed by the proposed VBI analysis for the car body of the vehicle traveling over a multi-unit horizontally curved simple bridge: the (a) lateral, (b) vertical, (c) rolling (d) yawing and (e) pitching accelerations.

4.3. Multi-span horizontally curved continuous bridges

This section examines the resonance condition of a multi-span horizontally curved continuous bridge under the passage of a series of (fifteen) vehicles (Fig. 11), which is common in railway engineering [23]. This section extends the work of Yang et al. [26] and Yau [27] by dealing with not only the vertical resonance, but also the lateral resonance of the continuous bridge. The effect of the number of spans on the resonance of the continuous bridge is also discussed.

Consider a horizontally curved continuous bridge of a single-line railway with the properties [28]: Young's modulus $E = 35.50$ GPa, mass per unit length $m = 11.69$ t/m, flexural moment of inertia $I_{yy} = 10.56$ m^4 in the lateral direction, and $I_{zz} = 6.78$ m^4 in the vertical direction, torsional constant $J = 17.34$ m^4, and length of each unit span $L^B = 56$ m. Three continuous bridges with different

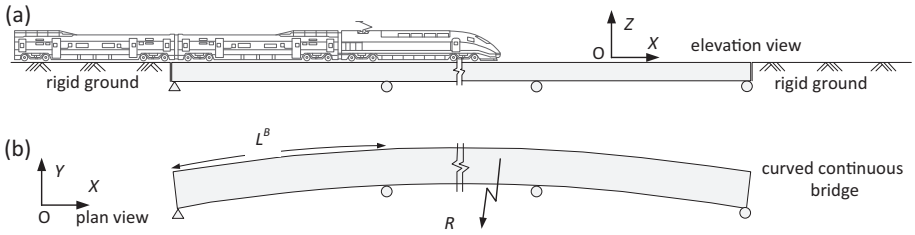

Fig. 11. Multi-span horizontally curved continuous bridges subjected to a series of vehicles.

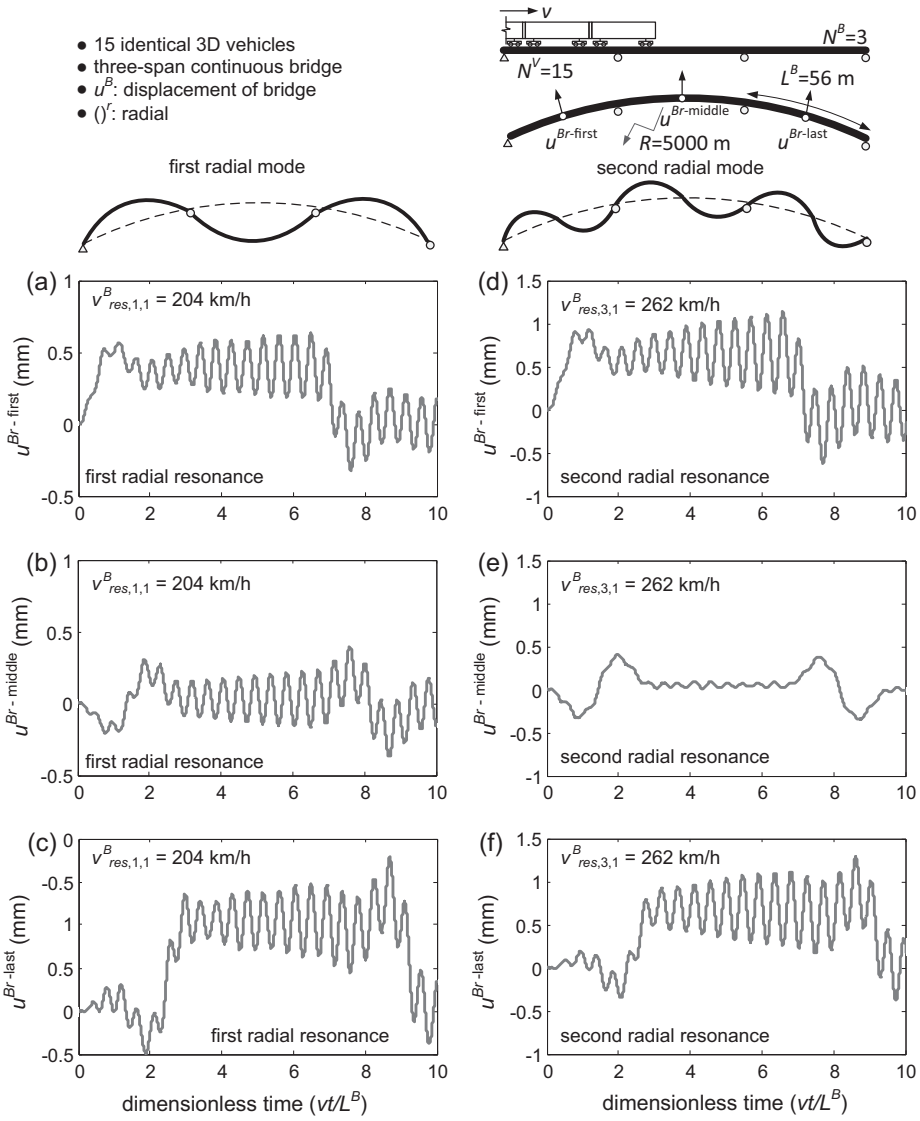

Fig. 12. Radial resonance displacement time histories of the first, middle and last span of a three-span continuous bridge, induced by the passage of fifteen identical vehicles, for the first (a), (b) and (c) and second (d), (e) and (f) radial modes.

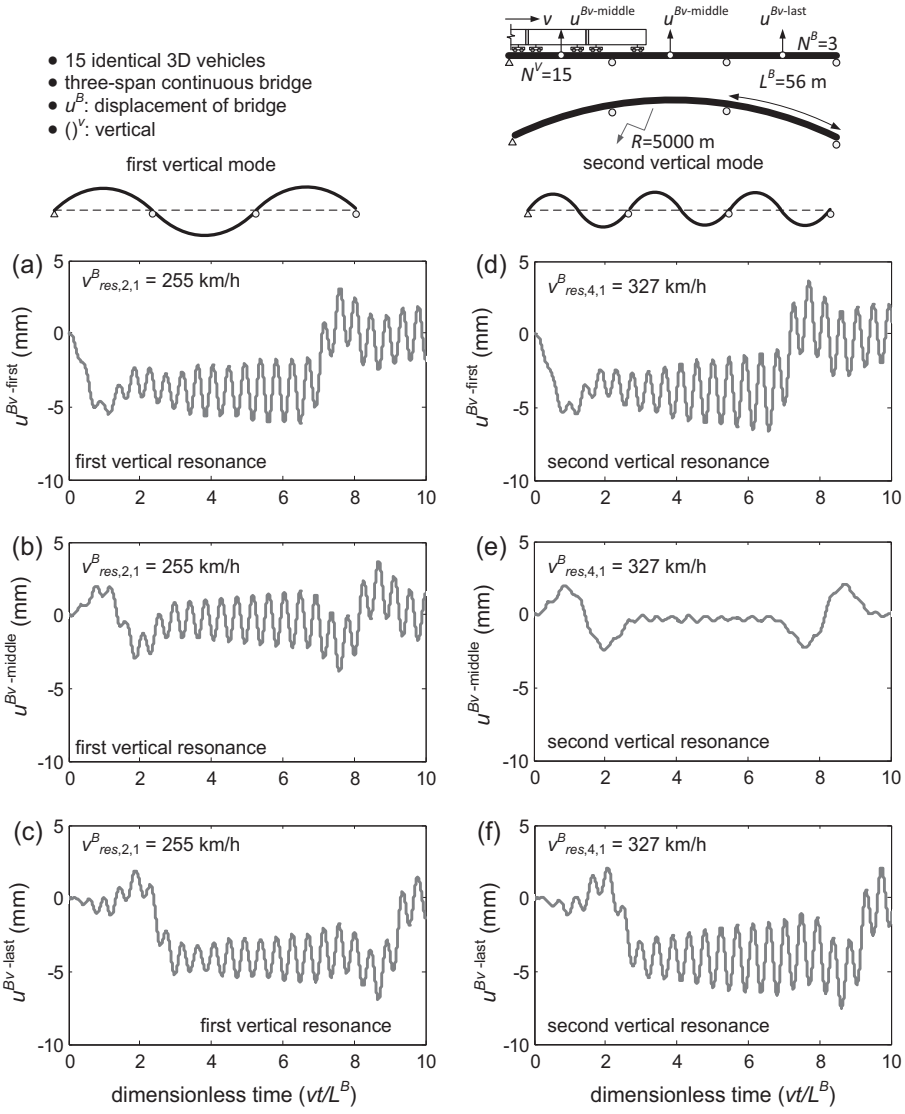

Fig. 13. Vertical resonance displacement time histories of the first, middle and last span of a three-span continuous bridge, induced by the passage of fifteen identical vehicles, for the first (a), (b) and (c) and second (d), (e) and (f) vertical modes.

Table 2
Natural frequencies and vibration modes of uniform continuous bridges.

	n = 1	2	3	4	5	6	7	8
Three-span								
f^B_n *hinged restraints*	2.28 (lateral)	2.84 (vertical)	2.92 (lateral)	3.64 (vertical)				
$v^B_{res,n,1}$ (km/h)	204	255	262	327				
f^B_n *free-mid restraints*	*0.28 (lateral)*	*1.02 (lateral)*	*2.28 (lateral)*	*2.84 (vertical)*				
$v^B_{res,n,1}$ (km/h)	*25*	*92*						
Five-span								
f^B_n *hinged restraints*	2.28 (lateral)	2.52 (lateral)	2.84 (vertical)	3.14 (vertical)	3.16 (lateral)	3.93 (vertical)		
$v^B_{res,n,1}$ (km/h)	204		255		284	354		
f^B_n *free-mid restraints*	*0.16 (lateral)*	*0.42 (lateral)*	*0.60 (lateral)*	*1.48 (lateral)*	*2.28 (lateral)*	*2.84 (vertical)*		
$v^B_{res,n,1}$ (km/h)	*14*	*38*	*54*					
Seven-span								
f^B_n *hinged restraints*	2.28 (lateral)	2.41 (lateral)	2.76 (lateral)	2.84 (vertical)	2.99 (vertical)	3.26 (lateral)	3.44 (vertical)	3.85 (lateral)
$v^B_{res,n,1}$ (km/h)	204		248	255			310	
f^B_n *free-mid restraints*	*0.13 (lateral)*	*0.28 (lateral)*	*0.51 (lateral)*	*0.83 (lateral)*	*1.23 (lateral)*	*1.70 (lateral)*	*2.28 (lateral)*	*2.84 (vertical)*
$v^B_{res,n,1}$ (km/h)	*12*	*25*	*46*					

numbers of spans, i.e. three, five, and seven spans, are examined. The boundary conditions at all supports are assumed as follows (Figs. 12 and 13): the longitudinal, the vertical and the radial displacement DOFs and the torsional rotation DOF are restricted, while the rotational (flexural) DOFs along the vertical and the radial direction are free. Table 2 lists the frequencies and the associated modes of the three continuous bridges. The fundamental frequencies of the bridge in the lateral and the vertical directions are 2.28

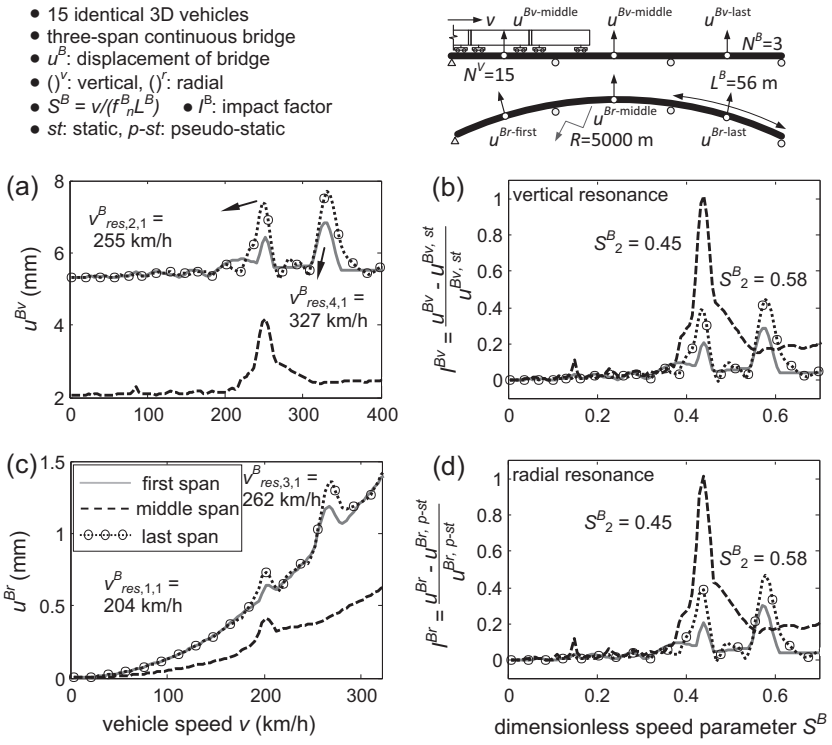

Fig. 14. Displacement response computed by the VBI analysis for the midpoint of different spans of a three-span continuous bridge subjected to fifteen identical vehicles: (a) and (b) vertical, (c) and (d) radial direction; (a) and (c) dimensional, (b) and (d) dimensionless response.

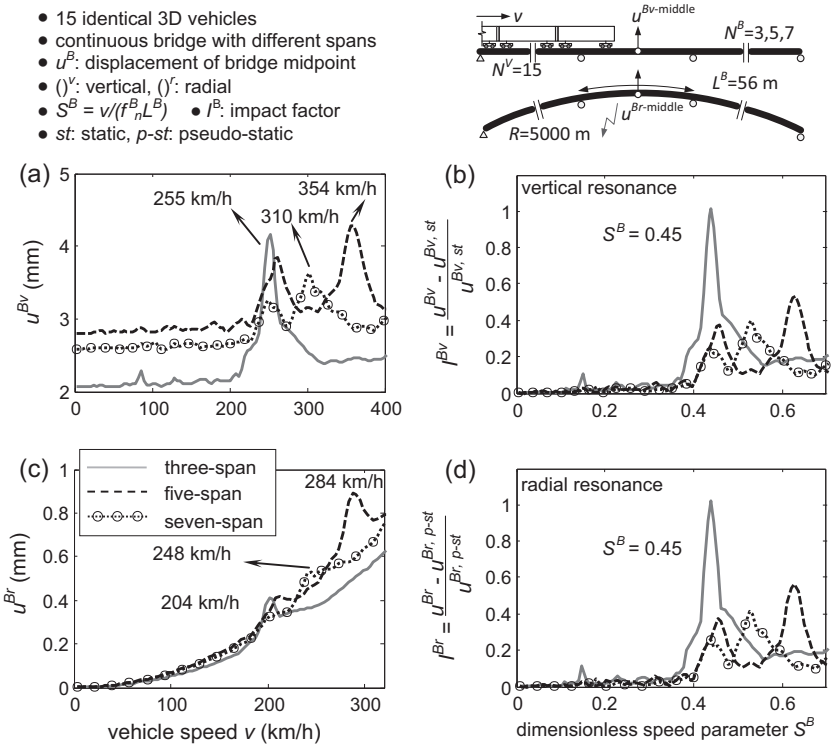

Fig. 15. Displacement response computed by the VBI analysis for the midpoint of the middle span of continuous bridge with different numbers of spans subjected to fifteen identical vehicles: (a) and (b) vertical, (c) and (d) radial direction; (a) and (c) dimensional, (b) and (d) dimensionless response.

and 2.84 Hz, respectively, irrelevant of the number of spans. The critical vehicle speeds in Table 2 are computed from Eq. (17).

Figs. 12 and 13 plot the radial and the vertical displacement time histories of the first, middle and last span of the three-span continuous bridge in resonance, respectively. When the bridge is in resonance, the displacements of the first, middle and last spans in the radial and the vertical directions keep increasing as more vehicles travel over the pertinent spans (resonance). The resonance speeds in Figs. 12 and 13 all agree well with the analytical values given in Table 2. Interestingly, for the second mode, no resonance occurs for the middle span (Figs. 12e and 13e). Recall that [27], the inflection point for the second mode of a three-span continuous bridge is the midpoint of the middle span; hence there is no contribution of the second mode to the resonance vibration of the midpoint of the three-span continuous bridge (see Figs. 12 and 13).

Fig. 14 plots the effect of vehicle speed on the displacement time histories of different points of a three-span continuous bridge, in both dimensional terms and dimensionless terms. For the first and the last spans two peaks appear in the vicinity of resonance in the vertical direction (255 and 327 km/h in Fig. 14a) and in the radial direction (204 and 262 km/h in Fig. 14c), which again agree well with the speeds of Table 2. On the contrary, for the middle span only one peak occurs (255 km/h Fig. 14). In other words, no resonance of the middle span occurs for the second mode in the vertical direction (Fig. 13a) and in the radial direction (Fig. 14c), which has also been explained in Figs. 12 and 13. When expressed in the dimensionless speed parameter S^B, the vertical and the radial dimensionless displacement time histories (impact factors) reveal a coincident first resonance speed parameter of $S_1^B = 0.45$, for the considered car length $d^V = 25$ m and span length $L^B = 56$ m. The second resonance peak $S_2^B = S_1^B \cdot f_2/f_1 = 0.45 \cdot 1.28 = 0.58$ corresponds to the second mode.

Fig. 14 also shows the differences between the displacements of different spans of the three-span continuous bridge. The resonance speeds are the same for the three different spans, both in the vertical and the radial directions. The middle span yields smaller dimensional displacements (Fig. 14a and c), but larger dimensionless displacements (Fig. 14b and d), compared with the same displacements of the first and the last spans. Due to the symmetry of the continuous bridge, the first and the last spans exhibit similar displacement pattern, both in dimensional and dimensionless terms.

Fig. 15 compares the resonance conditions of continuous bridges with different numbers of spans, i.e., three, five, and seven spans. Again, the resonance speeds of the continuous bridges agree well with the analytical ones given in Table 2. For continuous bridges with the same characteristic span L^B, the first critical resonance speeds are the same, regardless the number of spans. The increase in the number of spans makes the distribution of frequencies denser [27]. In Fig. 15, more peaks appear for continuous bridges with seven and five spans than with three spans. The

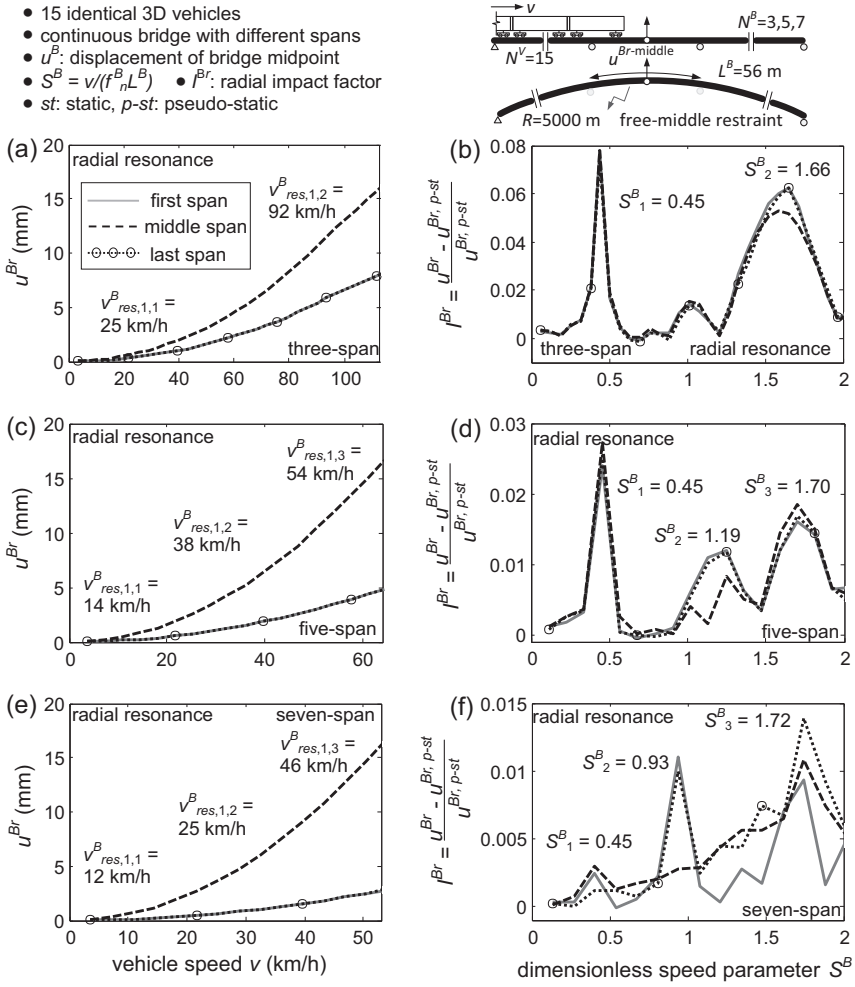

Fig. 16. Radial displacement response computed by the VBI analysis for the midpoint of different spans of continuous bridge with different numbers of spans subjected to fifteen identical vehicles: (a) and (b) three-span, (c) and (d) five-span and (e) and (f) seven-span, (a), (c) and (e) dimensional, (b), (d) and (f) dimensionless response.

increase of the number of spans results in both smaller dimensional displacement and lower dimensionless impact factor. The more spans a continuous bridge has, the more vibration energy, excited by the vehicular loads, is transferred to the adjacent spans, and therefore vibration is diminished [27].

Finally, Fig. 16 revisits the behavior of the three, five and seven-span continuous bridges of Figs. 12–15 for different support conditions. Specifically, it is assumed that the radial displacement is free at all middle supports. Hence, in the radial direction, the bridges are hinged at their end-supports, but free to translate at all middle supports. This reduces significantly their lateral stiffness and the frequencies of the lateral modes (*italic values* in Table 2). Again, the critical speeds at the radial spectra of Fig. 16 agree well with the analytical ones given in Table 2. Note that, while the difference in boundary condition reduces the dimensional critical speeds of bridge resonance, the dimensionless critical speed parameters remains the same in value (i.e. 0.45 in Fig. 16).

5. Conclusions

This study investigates the resonance behavior of the interacting vehicle-bridge system with the proposed 3D vehicle-bridge-interaction analysis approach. The simultaneous response of the vehicle and the bridge is captured under the resonance conditions of both the vehicle and the sustaining bridge.

The critical vehicle speeds from the proposed numerical resonance analysis scheme agree well with the analytical predicted values for the resonance of bridges, the cancelation of bridges and the resonance of vehicles. The critical vehicle speed in the equation for predicting the bridge resonance (Eq. (17)) is not directly affected by the span length of the bridge. As verified by the numerical study, the equation is not only applicable to simply supported bridges, but also to other types of bridges, like the continuous bridges with uniform span length.

The accumulated vibrations of the bridge under the bridge resonance conditions have a pronounced effect on the response of the running train vehicles. When a bridge is set in resonance, the later the vehicle enters the bridge, the higher the amplification of the acceleration of the vehicle sustained by the bridge.

The presence of damping in the suspension system prevents the resonance response of the car body to build up, even when the resonance condition of the vehicle is met. The vehicle's lateral-rolling and yawing resonance slightly amplifies the radial displacements of the later spans of the multi-unit bridge. The vehicle's vertical and pitching resonances have marginal effect (of second-order) on the vertical displacements of the bridge.

For simple bridges, the dimensional vertical displacement of the midpoint of the bridge is not affected by the radius of the curved bridge. The dimensional radial displacement of the midpoint of the bridge increases with the increase of the speed of the vehicle, but deceases with the increase of the radius of the curved bridge. The spectra of the dimensionless impact factors against the proposed dimensionless speed parameter in the vertical and the radial directions display the same pattern. The resonances of the bridges reveal a coincident resonance speed parameter in the vertical and the radial directions. The dimensionless impact factor spectra in the radial direction collapse to a single curve for different radii of the bridge.

For continuous bridges with the same length for each span, the critical speeds for the first resonance to occur are the same, both in the vertical and the radial directions. No resonance of the middle span of occurs for the second mode. The first and last spans exhibit similar displacement pattern, both in dimensional and dimensionless terms. The increase in the number of spans makes the distribution of resonances denser, which results in both smaller dimensional displacement and dimensionless impact factor. The free-to-translate condition for the radial direction at all middle supports of the continuous bridges reduces the dimensional critical speed of bridge resonance.

Acknowledgements

The second author likes to acknowledge of the sponsorship from the Chongqing Science & Technology Commission via the Contract Number of CSTC 2015 JCY JYS 30003 and the Tongji University 973 project with Grant No. 2011CB013800.

References

[1] Yang YB, Yau JD, Hsu LH. Vibration of simple beams due to trains moving at high speeds. Eng Struct 1997;19:936–44.
[2] Yang YB, Wu YS, Yao ZD. Vehicle-bridge interaction dynamics:with applications to high-speed railways. Singapore: World Scientific; 2004.
[3] Yau JD, Yang Y, Kuo S. Impact response of high speed rail bridges and riding comfort of rail cars. Eng Struct 1999;21:836–44.
[4] Yau JD, Wu YS, Yang YB. Impact response of bridges with elastic bearings to moving loads. J Sound Vibrat 2001;248:9–30.
[5] Yang YB, Lin CL, Yau JD, Chang DW. Mechanism of resonance and cancellation for train-induced vibrations on bridges with elastic bearings. J Sound Vibrat 2004;269:345–60.
[6] Xia H, Zhang N, Guo W. Analysis of resonance mechanism and conditions of train-bridge system. J Sound Vibrat 2006;297:810–22.
[7] Xia H, Li H, Guo WW, De Roeck G. Vibration resonance and cancellation of simply supported bridges under moving train loads. J Eng Mech 2013;140:04014015.
[8] Xia H, De Roeck G, Goicolea JM. Bridge vibration and controls: new research. Nova Science Publisher's; 2012.
[9] Song MK, Noh HC, Choi CK. A new three-dimensional finite element analysis model of high-speed train-bridge interactions. Eng Struct 2003;25:1611–26.
[10] Ju SH, Lin HT. Numerical investigation of a steel arch bridge and interaction with high-speed trains. Eng Struct 2003;25:241–50.
[11] Yau JD, Frýba L. Response of suspended beams due to moving loads and vertical seismic ground excitations. Eng Struct 2007;29:3255–62.
[12] Frýba L. A rough assessment of railway bridges for high speed trains. Eng Struct 2001;23:548–56.
[13] Cheng YS, Au FTK, Cheung YK. Vibration of railway bridges under a moving train by using bridge-track-vehicle element. Eng Struct 2001;23:1597–606.
[14] Dinh VN, Kim KD, Warnitchai P. Dynamic analysis of three-dimensional bridge-high-speed train interactions using a wheel-rail contact model. Eng Struct 2009;31:3090–106.
[15] Yang YB, Wu CM, Yau JD. Dynamic response of a horizontally curved beam subjected to vertical and horizontal moving loads. J Sound Vibrat 2001;242:519–37.
[16] Yang YB, Lin BH. Vehicle-bridge interaction analysis by dynamic condensation method. J Struct Eng 1995;121:1636–43.
[17] Yang YB, Yau JD. Vertical and pitching resonance of train cars moving over a series of simple beams. J Sound Vibrat 2015;337:135–49.
[18] Shabana AA, Zaazaa KE, Sugiyama H. Railroad vehicle dynamics: a computational approach. New York: CRC Press; 2010.
[19] Antolín P, Zhang N, Goicoleaa JM, Xia H, Astiza MÁ, Olivaa J. Consideration of nonlinear wheel-rail contact forces for dynamic vehicle-bridge interaction in high-speed railways. J Sound Vibrat 2013;332:1231–51.
[20] Dimitrakopoulos EG, Zeng Q. A three-dimensional dynamic analysis scheme for the interaction between trains and curved railway bridges. Comput Struct 2015;149:43–60.
[21] Cook RD. Concepts and applications of finite element analysis. New York: Wiley; 2007.
[22] Yang YB, Liao SS, Lin BH. Closure of "Impact formulas for vehicles moving over simple and continuous beams". J Struct Eng 1997;123(4):533–4.
[23] Yan B, Dai GL, Hu N. Recent development of design and construction of short span high-speed railway bridges in China. Eng Struct 2015;100:707–17.
[24] Wikipedia. Danyang-Kunshan Grand Bridge; 2015. <http://en.wikipedia.org/wiki/Danyang%E2%80%93Kunshan_Grand_Bridge>.
[25] Zeng Q, Dimitrakopoulos EG. Seismic response analysis of an interacting curved bridge-train system under frequent earthquakes. Earthquake Eng Struct Dyn 2015. http://dx.doi.org/10.1002/eqe.2699.
[26] Yang YB, Liao SS, Lin BH. Impact formulas for vehicles moving over simple and continuous beams. J Struct Eng 1995;121:1644–50.
[27] Yau JD. Resonance of continuous bridges due to high speed trains. J Mar Sci Technol 2001;9:14–20.
[28] Ding MB, Chen XC, Wang KZ. Self-vibration characteristic test of continuous curved railway bridge by means of environment random excitation. J Lanzhou Jiaotong Univ 2008;27:18–21 [In Chinese].